Available online at www.sciencedirect.com
ScienceDirect
Biosensors and Bioelectronics 23 (2008) 1244–1249
BIOSENSORS & BIOELECTRONICS
www.elsevier.com/locate/bios

Bioconjugation of zirconium uridine monophosphate: Application to myoglobin direct electrochemistry

Yuanbiao Qiao [a], Fangfang Jian [a,*], Qian Bai [b]

[a] *New Materials & Function Coordination Chemistry Laboratory, Qingdao University of Science and Technology, 266042 Qingdao Shandong, PR China*
[b] *Institution of Chemistry and Engineering, Qingdao University of Science and Technology, 266042 Qingdao Shandong, PR China*

Received 5 July 2007; received in revised form 12 November 2007; accepted 21 November 2007
Available online 28 November 2007

Abstract

Porous nano-granule of zirconium uridine monophosphate, $Zr(UMP)_2{\cdot}H_2O$ is, for the first time, synthesized under mild experimental conditions and applied to the bioconjugation of myoglobin (Mb) to realize its direct electron transfer. UV–vis and resonance Raman spectroscopies prove that Mb in the $Zr(UMP)_2{\cdot}H_2O$ film maintains its secondary structure similar to the native state. The conjugation film of the Mb–$Zr(UMP)_2{\cdot}H_2O$ on the glassy carbon (GC) electrode gives a well-defined and quasi-reversible cyclic voltammogram, which reflects the direct electron transfer of the heme Fe^{III}/Fe^{II} couple of Mb. On the basis of the satisfying bioelectrocatalysis of the nano-conjugation of Mb and genetic substrate, a kind of mediator-free biosensor for H_2O_2 is developed. The linear range for H_2O_2 detection is estimated to be 3.92–180.14 μM. The apparent Michaelis–Menten constant (K_m) and the detection limit based on the signal-to-noise ratio of 3 are found to be 196.1 μM and 1.52 μM, respectively. Both the apparent Michaelis–Menten constant and the detection limit herein are much lower than currently reported values from other Mb films. This kind of sensor possesses excellent stability, long-term life (more than 20 days) and good reproducibility.

Keywords: Myoglobin; $Zr(UMP)_2{\cdot}H_2O$; Bioconjugation; Direct electrochemistry; H_2O_2 biosensor

1. Introduction

The development of materials science has brought about a great momentum to bioelectroanalysis (Cai et al., 2006). Analysts in this field are always enthusiastic in finding new materials with good biocompatibility to improve the behavior of biosensors. Nanomaterials of metal oxides can be used as effective supports for enzymes loading (Topoglidis et al., 2003; Cao and Hu, 2006; Salimi et al., 2006; Liu et al., 2005; Liu and Hu, 2005; Peng et al., 2004; Yap and Zhang, 2007; Zhou et al., 2006) and have already been widely used in biosensor fabrication (Topoglidis et al., 2003; Cao and Hu, 2006; Salimi et al., 2006; Liu et al., 2005; Liu and Hu, 2005; Peng et al., 2004). Recently, porous nanomaterials of arrayed microstructure have made great contributions to the areas such as biosensor, drug deliver, micro-reactor, and bio-separation (Shchukin et al., 2004; Zhu et al., 2005).

Nanoparticle of zirconia has been extensively applied to the study on proteins consolidation (Zhao et al., 2005; Liu et al., 2004). It can provide a good compatible microenvironment to prevent proteins from aggregating and spontaneous denaturating to a significant extent, and an access to the immobilized proteins for cofactors, substrates, or redox reagents (Rosevear et al., 1987). The porous material of zirconium phosphate is used as the support matrix for proteins loading due to the distinctive characteristics of the layered microstructure with hydrophilic hydroxyl groups on the two-dimensional lamellar surface (Kumar and McLendon, 1997; Kumar and Chaudhari, 2000, 2003). The interlayers can be readily expanded to accommodate guest proteins. Proteins immobilized in the interlayers of the zirconium phosphonates have also been studied (Kumar and Chaudhari, 2003, 2001; Bellezza et al., 2004). Proteins in these materials retain their conformations similar to the native states at room temperature. However, the thermal stability and the refolding

* Corresponding author. Tel.: +86 532 84023606; fax: +86 532 84023606.
E-mail address: ffj2003@163169.net (F. Jian).

0956-5663/$ – see front matter © 2007 Elsevier B.V. All rights reserved.
doi:10.1016/j.bios.2007.11.008

efficiency after thermal denaturation of the bound proteins vary greatly owing to the surface functions of these materials. The hydrophilic nature on the surface plays an important role in stabilizing the bound proteins (Kumar and Chaudhari, 2000).

Based on the development of the new zirconium material for the purpose of protein consolidation with intensifying performances, zirconium uridine monophosphate, $Zr(UMP)_2{\cdot}H_2O$, has been designed and prepared in suspension. This compound is interesting for its combinatorial advantages inherited from the parent materials. Water-soluble polyions of nucleic acids have been designed for specific molecular architectural plans (Lvov et al., 1993; Ferreira and Rubner, 1995; Hammond, 1995; Lvov et al., 1998). Chemistry of the proteins in the functional films of nucleic acids has also been explored, which reveals that proteins undergo absolutely compatible adsorption (Lvov et al., 1998). As a component of nucleic acid, the UMP motif in $Zr(UMP)_2{\cdot}H_2O$ is proposed to have much recognition cofactor to protein binding than other polyions, such as surfactant, polyallylamine, polythiophene-3-acetic acid, polyallylamine hydrochloride/sulfonated polystyrene, and polydiallyldimethylammonium chloride/sulfonated polystyrene. The zirconium material provides as an ideal template in protein immobilization owing to its inherent characteristics such as non-toxicity, chemical inertness and negligible swelling in aqueous solution (Kumar and Chaudhari, 2000). In addition, the morphology of the porous nano-granules of $Zr(UMP)_2{\cdot}H_2O$ is superior in the design of biosensor and biomedical device because of the unique properties that stems from the high surface-to-volume ratio and the spatial charge carrier confinement (Trindade et al., 2001; Zhang, 2000). However, as far as we know, the electrochemistry of the proteins in the film of $Zr(UMP)_2{\cdot}H_2O$ has never been reported.

Herein, met-myoglobin (Mb) is conjugated to the porous nano-granules of $Zr(UMP)_2{\cdot}H_2O$, and the conjugation film is then fabricated on the glassy carbon (GC) electrode, using cetyl trimethylammonium bromide (CTAB) as a linker. A pair of well-defined and nearly symmetric redox peaks is achieved, which reflects the facile and quasi-reversible electron transfer between Mb and the GC electrode. The conformation of the conjugated Mb retains its native structure as characterized by UV–vis and resonance Raman spectroscopies. The Mb–$Zr(UMP)_2{\cdot}H_2O$ film on the GC electrode is sensitive to the electrocatalytic reduction of H_2O_2, showing the potential application as a foundation of third-generation biosensor or bioreactor.

2. Experimental section

2.1. Chemicals and apparatus

Lyophilized met-Mb (MW 17,800, Sigma) from horse heart is used as received. The stock solution (1.0 mM Mb in the pH 7.0 buffer) is stored at 4 °C. The 0.1 M phosphate buffers of different pH values are prepared with the mixtures of the Na_2HPO_4 and NaH_2PO_4 solutions, and then adjusted with 0.1 M H_3PO_4 or NaOH. Diluted H_2O_2 (30% (w/w), Beijing Chemical Plant) solutions are prepared daily. Other chemicals are of analytical grade. All solutions are prepared with re-distilled water.

$Zr(UMP)_2{\cdot}H_2O$ is prepared with the following procedures: 0.1 mmol $UMPNa_2$ (Serve product) is dissolved in a volume of 100 ml of cetyl trimethylammonium bromide (CTAB, 0.1% (w/w)) aqueous solution. Then, a volume of 10 ml of 5 mM $ZrCl_4$ (Merck–Schuchardt product) aqueous solution is dropwise added to above solution within 10 min. The translucent suspension is formed in a period of 10 h fleet stirring (8000 r/min) at 4 °C. It is then centrifuged and washed three times with ethanol. Finally, the product of $Zr(UMP)_2{\cdot}H_2O$ is dried in vacuum.

Elemental analysis (EA) of $Zr(UMP)_2{\cdot}H_2O$ is performed using a PekinElmer analyzer (1400 C). The morphology is determined by a field-emission scanning electron microscopy (FE-SEM, JSM 6700F). UV–vis absorption spectra of the dry films of $Zr(UMP)_2{\cdot}H_2O$, Mb and Mb–$Zr(UMP)_2{\cdot}H_2O$ are checked on a CARY-500 spectrophotometer by using the quartz slides. Resonance Raman spectra of the thin films of Mb and Mb–$Zr(UMP)_2{\cdot}H_2O$ on the silica wafers (after being dried at room temperature) are obtained with a 406.7 nm laser line as the excitation source (Spectra-Physics model 2080 KV). The spectra are recorded on a 0.6 m triple spectrometer (Spex model 1877) with a charge-coupled device (CCD) (Feng and Tachikawa, 2001). A 1200 line/mm grating is selected for the experiments. Electrochemical measurements are performed on an Autolab PGSTAT-30 digital potentiostat/galvanostat, (Eco Chemie BV, Utrecht, Netherlands). A three-electrode system is used with the Mb–$Zr(UMP)_2{\cdot}H_2O$ film-coated the glassy carbon (GC) electrode as the working electrode, a platinum sheet (0.8 cm × 0.8 cm) as the auxiliary electrode, and an Ag/AgCl (1.0 M KCl) electrode as the reference one. All the potentials reported in this work are in reference to the value of this electrode (236.3 mV at 20 °C). All electrochemical measurements are carried out in 0.1 M anaerobic phosphate buffers at 20 ± 2 °C.

2.2. Electrode modification

The basal plane GC (ϕ 2 mm) electrode is polished with 1.0 μm, 0.3 μm and 0.05 μm alumina slurries, respectively, washed and further sonicated in re-distilled water. A volume of 2 μl of the aqueous composite made from 0.5 mM Mb and 0.1 mg ml^{-1} $Zr(UMP)_2{\cdot}H_2O$ in 0.1% CTAB (after ultrasonication for 15 min) is uniformly coated onto the inverted GC electrode surface. In a similar way, the matrix-only coated electrode is prepared by syringing a volume of 2 μl of 0.1 mg ml^{-1} $Zr(UMP)_2{\cdot}H_2O$ in 0.1% CTAB aqueous solution on the electrode surface. These electrodes are then dried under ambient conditions before being used.

3. Results and discussions

3.1. $Zr(UMP)_2{\cdot}H_2O$ characterizations

$Zr(UMP)_2{\cdot}H_2O$ is precipitated into white powder. EA (%) results are C 26.10, H 3.44 and N 6.78, respectively, which are well correlated with the theoretical values of C 26.09, H 3.41 and N 6.76 for $Zr(UMP)_2{\cdot}H_2O$. Solid UV–vis spectrum of

$Zr(UMP)_2{\cdot}H_2O$ gives an intraligand (IL) π–π* transition (Juris et al., 1988) band at λ_{max} 265 nm, which red-shifts 5 nm in comparison with the free UMP. The infrared spectrum shows the vibration bands of P–O–C 999 cm^{-1}, P=O 1170 cm^{-1}, C=N 1592 cm^{-1} and C–N–H 1720 cm^{-1}, respectively. The strong band of the C–N–H vibration shifts 22 cm^{-1} in the direction of high-frequency when compared with that of the free UMP at 1698 cm^{-1}. UV–vis and infrared spectroscopic results indicate the coordination between Zr atom and the N atom from the heterocyclic UMP. The low-magnification SEM image reveals that $Zr(UMP)_2{\cdot}H_2O$ is entirely composed of nanospheres with a well-ordered and porous morphology. The maximum dimension of these granules is estimated to be 100 nm from its high-magnification SEM image.

3.2. Spectroscopic characterizations of the Mb–Zr(UMP)$_2$·H$_2$O film

The position of the Soret absorption band provides the information about possible denaturation of heme proteins, especially that of conformational change in the heme group region (George and Hanania, 1953; Antonini and Brunori, 1971). Thus, UV–vis spectroscopy is a useful tool for the conformational study of heme proteins. Fig. 1 shows UV–vis spectra of the dry films of free Mb and Mb–$Zr(UMP)_2{\cdot}H_2O$. The Soret band for the Mb–$Zr(UMP)_2{\cdot}H_2O$ film is located at 412 nm, essentially the same as that obtained from free Mb. These results suggest that there is no denaturation for conjugated Mb in the film.

The CTAB surfactant in the microemulsion solution induces stabilizing and promoting the heme proteins (Nadzhafova et al., 2004; Nuthakki and Rusling, 2005). The Soret absorption of the aqueous composite made from 0.5 mM Mb and 0.1 mg ml^{-1} $Zr(UMP)_2{\cdot}H_2O$ decreases by about 2% with the increasing the CTAB concentration from 0.00 mg ml^{-1} to 0.35 mg ml^{-1}. Meanwhile, the position of the Soret band gives no change from that of the composite without the surfactant. These results reveal

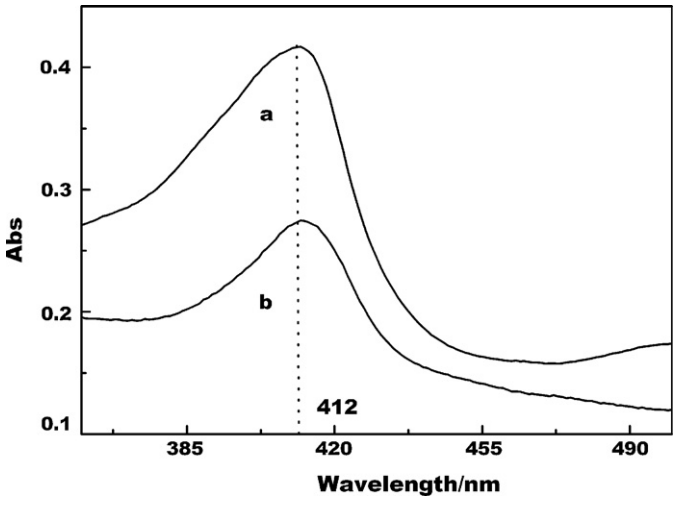

Fig. 1. UV–vis spectra of (a) the Mb and (b) the Mb–$Zr(UMP)_2{\cdot}H_2O$ films. Samples were prepared by coating 0.1 ml of 0.5 mM Mb, and the composite of 0.5 mM Mb and 0.1 mg ml^{-1} $Zr(UMP)_2{\cdot}H_2O$ in 0.1% CTAB aqueous solutions, respectively on the quartz slides (1.0 cm × 1.0 cm) and air-dried overnight.

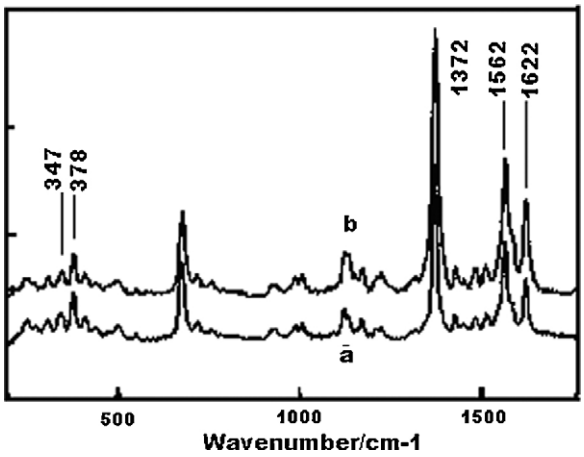

Fig. 2. Resonance Raman spectra of (a) the Mb and (b) the Mb–$Zr(UMP)_2{\cdot}H_2O$ dry films on the silica wafers. Samples were prepared in the same method as those in Fig. 1.

that the protein herein is mostly stabilized by the $Zr(UMP)_2{\cdot}H_2O$ bioconjugator.

Vibration spectroscopy is a sensitive technique to probe into the secondary structure of proteins. The profiles of the amide I and amide II provide detailed information about the secondary structure of the polypeptide chain (Kauppinen et al., 1981). Fig. 2 presents resonance Raman spectra of Mb and the Mb–$Zr(UMP)_2{\cdot}H_2O$ films. Shapes of the amide I and the amide II bands at 1622 cm^{-1} and 1562 cm^{-1} for the Mb–$Zr(UMP)_2{\cdot}H_2O$ film are similar to those of the pure Mb film. The marker bands corresponding to oxidation and spin states of heme iron (Feng and Tachikawa, 2001) are located at 1372 cm^{-1} and 1562 cm^{-1} for both the free Mb and the Mb–$Zr(UMP)_2{\cdot}H_2O$ films. In the low-frequency region, the Raman bands for vibration modes of the Fe–N stretching and the heme deforming (Desbois et al., 1979) are all located at 378 cm^{-1} and 347 cm^{-1}. These results further confirm that $Zr(UMP)_2{\cdot}H_2O$ actually provides a biocompatible microenvironment for Mb loading, and the secondary structure of the protein is undisturbed.

3.3. Electrochemical characterizations of the Mb–Zr(UMP)$_2$·H$_2$O film

Fig. 3 presents the overlapped cyclic voltammograms of the GC electrode coated with the Mb–$Zr(UMP)_2{\cdot}H_2O$ film at the scan rates (ν) from 0.01 Vs^{-1} to 0.1 Vs^{-1}. The electrode coated with the $Zr(UMP)_2{\cdot}H_2O$ film gives no redox peaks in both the pH 7.0 phosphate buffer and the Mb solution. However, well-defined and nearly symmetric cyclic voltammograms attributed to the heme Fe^{III}/Fe^{II} redox couple of Mb are observed on the GC electrodes coated with the Mb–$Zr(UMP)_2{\cdot}H_2O$ film in the pH 7.0 phosphate buffer. Differential pulse voltammograms also show symmetric redox waves with the same redox potential on this electrode. These results indicate that direct electron transfer between Mb and the GC electrode is achieved through the conjugation of Mb and $Zr(UMP)_2{\cdot}H_2O$. The formal potential ($E^{\circ\prime}$) defined as the average value of the anodic peak potential (E_{pa})

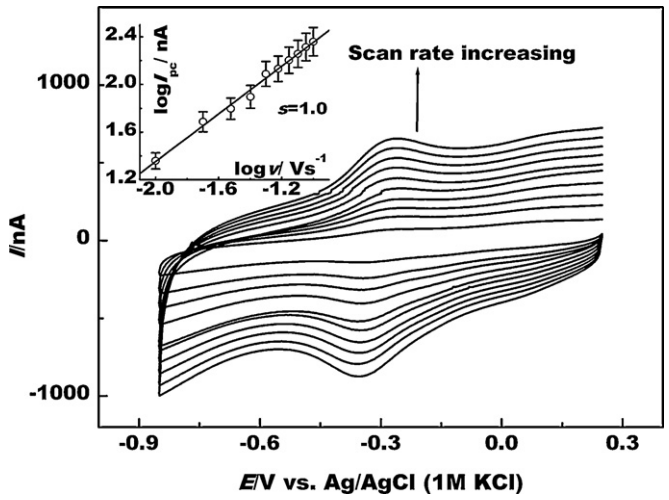

Fig. 3. Cyclic voltammograms of the GC electrode coated with the Mb–Zr(UMP)$_2$·H$_2$O film in the pH 7.0 phosphate buffer. The scan rates are 0.01–0.1 V s^{-1} (from inner to outer) at an interval of 0.01 V s^{-1}. Inset: plot of log I_{pc} vs. log υ.

and the cathodic peak potential (E_{pc}) is calculated to be −0.30 V, and the peak separation (ΔE_p) between E_{pa} and E_{pc} is 48 mV at the ν value of 0.01 V s^{-1}. Within the selected ν values from 0.01 V s^{-1} to 0.1 V s^{-1}, plot of logarithm of the cathodic currents (I_{pc}) obtained from cyclic voltammograms versus logarithm of the scan rates (ν) has a linear correlation with the regression coefficient and the slope (s) of 0.999 and 1.0, respectively (inset in Fig. 3). The slope is the same value for the theoretical thin-layer electrochemistry (Bard and Faulkner, 2001). These results suggest that all of the electroactive Mb Fe^{III} in the film is converted to Mb Fe^{II} on the forward scan to the negative potential, with full conversion of Mb Fe^{II} to Mb Fe^{III} on the reversed scan.

The average electroactive concentration (Γ^*) of Mb on the electrode surface, estimated with the relation (Bard and Faulkner, 2001): $Q = nFA\Gamma^*$ (Q, n, F, A represents the integrated charge, the electron transfer number, the Faraday's constant, and the electrode area, respectively), is calculated to be 2.93×10^{-10} mol cm^{-2} (here, $Q = 0.85$ μC at 0.01 Vs^{-1}, $A = 0.03$ cm^2 and $n = 1$ assumed). This value is about 10-fold larger than that of Mb in the nucleic acid film but close to Mb in other zirconium films (Lvov et al., 1998; Zhao et al., 2005). It is proposed that the hydrophilic groups of Zr(UMP)$_2$·H$_2$O promote binding and that the positive charges accelerate activating of Mb. Taking into account the amount of 0.47×10^{-10} mol cm^{-2} of the monomolecular layer (Lvov et al., 1998), and the crystallographic dimensions of 2.5 nm × 3.5 nm × 4.5 nm of Mb (Kendrew et al., 1960), we conclude that about six layers (∼27 nm) of the protein molecules close to the inner surface of the electrode keep electroactive.

At the ν values lower than 0.05 V s^{-1}, both the cathodic peak potential and the anodic peak potential are nearly constant, whereas the cathodic peak potential shifts negatively and the anodic peak potential shifts positively at the ν values above 0.05 V s^{-1}, which is consistent with the onset of kinetic control (Huang et al., 1996). The electron transfer rate coefficient (k_s) is obtained from the ΔE_p values in the range of the ν values for kinetic control. The derivate relation by (Laviron, 1979): $1/m = 1.459 \times 10^{-2} + 2.335 \times 10^{-2}\Delta E_p + 1.323 \times 10^{-4}\Delta E_p^2 + \cdots$, is used for $n\Delta E_p < 200$ mV. Here, $m = (RT/F)(k_s/n\nu)$ and $n = 1$ assumed. Thus, the average value of k_s for the Mb–Zr(UMP)$_2$·H$_2$O film on the GC electrode is obtained to be 1.1 ± 0.3 s^{-1}.

It is well known that the solutions pH modulate the accessibility of water to the heme pocket of Mb and the protonation of the heme iron bound proximal histidine and/or the distal histidine in the heme pocket. Consequently, cyclic voltammograms of the GC electrode coated with the Mb–Zr(UMP)$_2$·H$_2$O film show a strong dependence on the pH value of the external solutions. The increase in the pH from 4.0 to 11.0 leads to negative shifts in the potentials for both the cathodic peaks and the anodic peaks. Fig. 4 presents the relationship between $E^{\circ\prime}$ and pH. A linear regression yields the slope of 49.3 mV pH^{-1}, which suggests that the electron transfer between Mb and the GC electrode is coupled to proton transfer. This slope is slightly lower than the expected value of the heme iron redox (58.0 mV pH^{-1}, at 20 °C) for a single electron transfer (Bond, 1980). The slightly lower value may result from the protonation of the water molecule coordinated to the heme Fe^{III}, or from the protonation states of the *trans* ligands to the heme Fe^{III} and the amino acids around the heme group (Yamazaki et al., 1978).

The GC electrode coated with the Mb–Zr(UMP)$_2$·H$_2$O film is immersed in pH 7.0 phosphate buffer and stored at 4 °C. Cyclic voltammograms are obtained periodically to estimate the stability of conjugated Mb in the film. The peak heights of cyclic voltammograms decrease by about 8% within 30 days. Also, no more than 5% of Mb in the Zr(UMP)$_2$·H$_2$O film is desorbed during 20–30 voltammetric cycles. The effect of the CTAB surfactant on the Mb–Zr(UMP)$_2$·H$_2$O composite film-coated electrode has also been investigated. Experiments show that the Mb–Zr(UMP)$_2$·H$_2$O composite can be easily and steadily fabricated on the GC electrode with the aid of the CTAB cross-linker. Further studies confirm that there is no difference in the redox peak heights when the CTAB concentration is lower than

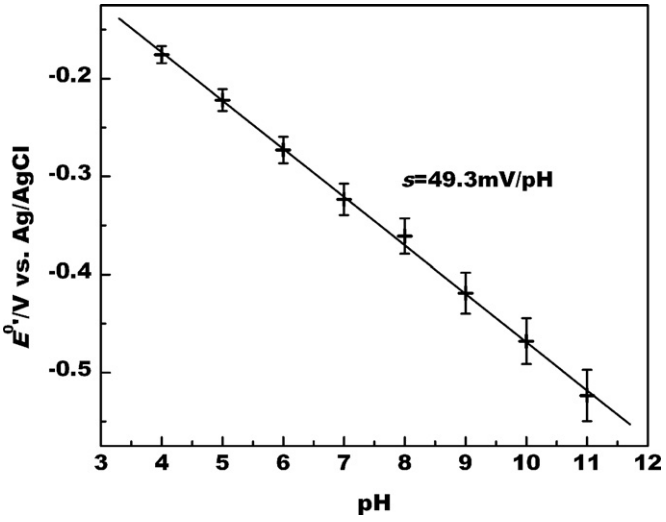

Fig. 4. Plot of formal potential ($E^{\circ\prime}$) vs. pH for the Mb–Zr(UMP)$_2$·H$_2$O film on the GC electrode in the pH 7.0 phosphate buffer.

0.35 mg ml^{-1}. Similar result has also been obtained previously (Nadzhafova et al., 2004), where the CTAB concentration was chosen to be less than 0.4 mg ml^{-1}.

3.4. Electrocatalytic properties of the Mb–Zr(UMP)$_2$·H$_2$O film

Cyclic voltammetric study of the Mb–Zr(UMP)$_2$·H$_2$O film-coated GC electrode in the presence of dissolved O_2 is performed. When the electrode is dipped into the O_2-saturated solution, only a large peak at about −0.28 V attributed to the Mb Fe^{III} reduction is observed in the pH 7.0 phosphate buffer, and the anodic peak for the oxidation of the Mb Fe^{II} is disappeared. However, a well-defined and nearly reversible redox couple is observed with almost equal heights of redox peaks when O_2 is carefully excluded. The reduction peak potential positively shifts by about 40 mV when O_2 is saturated. Results are consistent with the following three steps: initial reduction Mb Fe^{III} → Mb Fe^{II}, the reaction of the Mb Fe^{II} with O_2, and reduction of the Mb Fe^{II}–O_2 complex to give H_2O_2. The ratio of the cathodic peak currents in the presence (I_c) and in the absence of O_2 (I_d) decreases along with the increasing of the ν values, which is evidence for the electrocatalysis to the O_2 reduction (Andrieux et al., 1979). At the ν value of 0.01 V s^{-1}, the Mb–Zr(UMP)$_2$·H$_2$O film-coated GC electrode gives the I_c/I_d ratio of 86. This result indicates that the protein-catalyzed reduction of O_2 gives much H_2O_2, and Mb in the Zr(UMP)$_2$·H$_2$O film keeps a high enzymatic activity.

Cyclic voltammetry is also used to examine the electrocatalysis to the H_2O_2 reduction of this electrode (Fig. 5A). The cathodic peak at about −0.28 V for the Mb–Zr(UMP)$_2$·H$_2$O film on the GC electrode is greatly enhanced in the presence of H_2O_2, while the corresponding anodic peak is decreased. The anodic peak ultimately disappears when the concentration of H_2O_2 is increased. Within the selected potential window, the GC electrode coated with Zr(UMP)$_2$·H$_2$O alone gives no response in the presence of H_2O_2. These results indicate that an electrocatalysis to the H_2O_2 reduction occurs at the Mb–Zr(UMP)$_2$·H$_2$O composite film-coated electrode. The cathodic peak potential positively shifts by about 40 mV in the initial of the H_2O_2 reduction (curve b in Fig. 5A), showing a fast electrocatalytic behavior. Defined as the difference between the cathodic peak current (I_{pc}) in the presence of H_2O_2 and the I_{pc} in the absence of H_2O_2, the electrocatalytic current (I_{cat}) varies linearly with the H_2O_2 concentration in the beginning and thereafter levels off (Fig. 5B), which reveals that the Mb–Zr(UMP)$_2$·H$_2$O conjugation responds to the electrocatalytic reduction of H_2O_2 in a Michaelis–Menten model. The linear regression in the range of 3.92–180.14 μM H_2O_2 yields the equation: $I_{cat} = -0.59 + 2.36$ [H_2O_2], and the detection limit based on the signal-to-noise ratio of 3 is calculated to be 1.52 μM. The Lineweaver–Burke plot gives an apparent Michaelis–Menten constant (K_m) of 196.1 μM for the Mb–Zr(UMP)$_2$·H$_2$O film. In contrast with reported values from other Mb films (Liu et al., 2005; Liu and Hu, 2005; Peng et al., 2004; Shchukin et al., 2004; Liu et al., 2004; Bellezza et al., 2004), the analytical performances of the Mb–Zr(UMP)$_2$·H$_2$O film show lower detection limit, and smaller K_m except that reported by Liu and Hu (2005). Daily determination of cyclic voltammograms in H_2O_2 solutions shows that the enzyme-catalyzed reactivity of the Mb–Zr(UMP)$_2$·H$_2$O film keeps nearly the same level within 20 days. The analytic reproducibility of this H_2O_2 biosensor has been studied and the results are listed in Table 1. It gives the standard recovery ratio (%) of 91.26–106.08, and the relative standard derivation (R.S.D.%) of 0.59–3.23 within five parallel determinations when the H_2O_2 concentration is in the range of 4.00–175.00 μM.

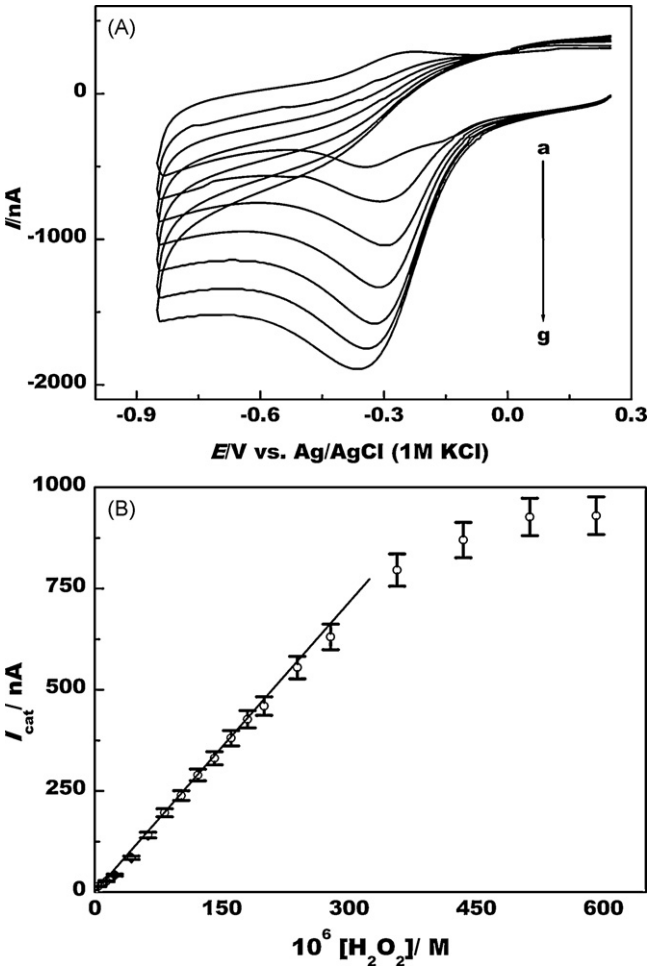

Fig. 5. (A) Cyclic voltammograms of the GC electrode coated with the Mb–Zr(UMP)$_2$·H$_2$O film in the pH 7.0 phosphate buffer in the presence of (a) 0.00, (b) 82.24, (c) 140.98, (d) 278.04, (e) 356.36, (f) 434.68 and (g) 591.32 μM H_2O_2. The scan rate was 0.035 V s^{-1}. (B) Typical plot of electrocatalytic current (I_{cat}) vs. [H_2O_2].

Table 1
H_2O_2 analytical application of the Mb–Zr(UMP)$_2$·H$_2$O film (n = 5)

[H_2O_2]$_{added}$ (μM)	[H_2O_2]$_{detected}$[a] (μM)	Recovery ratio (%)	R.S.D. (%)
4.00	4.02	91.26–105.42	3.23
20.00	19.97	94.46–97.38	2.25
75.00	75.12	95.00–103.34	0.59
125.00	125.53	93.16–99.82	1.14
175.00	173.87	92.22–106.08	2.63

[a] Average value of five times parallel determinations.

4. Conclusion

Facile electrochemistry of the Mb–$Zr(UMP)_2{\cdot}H_2O$ film on the GC electrode and the application to H_2O_2 biosensor have been reported in this work. The protein in this manner realizes absolutely biocompatible combination with $Zr(UMP)_2{\cdot}H_2O$ and then exerts facile direct electrochemistry with excellent stability and long-term life. It is proposed that the hydrophilic groups of $Zr(UMP)_2{\cdot}H_2O$ promote binding of Mb and that the positive surface charges accelerate activating. The conjugated Mb demonstrates satisfying protein-catalyzed reactivity to the reductions of O_2 and H_2O_2. Based on the direct electrochemistry of the bioconjugation of Mb with the nano-dimensional $Zr(UMP)_2{\cdot}H_2O$, the H_2O_2 biosensor realizes very low detection limit, high enzymatic activity and good reproducibility.

Acknowledgment

The authors thank Natural Science Foundation of Shandong Province (Grant No. Y2005B04) for the financial support.

Appendix A. Supplementary data

Supplementary data associated with this article can be found, in the online version, at doi:10.1016/j.bios.2007.11.008.

References

Andrieux, C.P., Blocman, C., Dumas-Bouchiant, J.M., Saveant, J.M., 1979. J. Am. Chem. Soc. 101 (13), 3431–3441.
Antonini, E., Brunori, M., 1971. Hemoglobin and Myoglobin in Their Reactions with Ligands. North-Holl, Amsterdam, p. 13.
Bard, A.J., Faulkner, L.R., 2001. Electrochemical Methods: Fundamentals and Applications. Wiley, New York.
Bellezza, F., Cipiciani, A., Costantino, U., Nicolis, S., 2004. Langmuir 20 (12), 5019–5025.
Bond, A.M., 1980. Modern Polarographic Methods in Analytical Chemistry. Dekker Marcel, New York, p. 27.
Cai, W.Y., Zhao, X.N., Zhu, J.J., Chen, H.Y., 2006. Chem. Mater. 18 (2), 279–284.
Cao, D.F., Hu, N.F., 2006. Biophys. Chem. 121 (3), 209–217.
Desbois, A., Lutz, M., Banerjee, R., 1979. Biochemistry 18 (8), 1510–1518.
Feng, M., Tachikawa, H., 2001. J. Am. Chem. Soc. 123 (13), 3013–3020.
Ferreira, M., Rubner, M.F., 1995. Macromolecules 28 (21), 7107–7114.
George, P., Hanania, G., 1953. Biochem. J. 55 (2), 236–243.
Hammond, P.T., 1995. Macromolecules 28 (22), 7569–7571.
Huang, Q., Lu, Z., Rusling, J.F., 1996. Langmuir 12 (22), 5472–5480.
Juris, A., Balzani, V., Barigelletti, F., Campagna, S., Belser, P., Zelewsky, A.V., 1988. Coord. Chem. Rev. 84, 85–277.
Kauppinen, J.K., Moffatt, D.J., Mantsch, H.H., Cameron, D.G., 1981. Appl. Spectrosc. 35 (3), 271–276.
Kendrew, J., Phillips, D., Stone, V., 1960. Nature 184, 422–429.
Kumar, C.V., Chaudhari, A., 2000. J. Am. Chem. Soc. 122 (5), 830–837.
Kumar, C.V., Chaudhari, A., 2001. Chem. Mater. 13 (2), 238–240.
Kumar, C.V., Chaudhari, A., 2003. Microporous Mesoporous Mater. 57 (2), 181–190.
Kumar, C.V., McLendon, G.L., 1997. Chem. Mater. 9 (3), 863–870.
Laviron, E., 1979. J. Electroanal. Chem. 101, 19–28.
Liu, H., Hu, N., 2005. J. Phys. Chem. B 109 (20), 10464–10473.
Liu, S.Q., Dai, Z.H., Chen, H.Y., Ju, H.X., 2004. Biosens. Bioelectron. 19 (9), 963–969.
Liu, A., Wei, M., Honma, I., Zhou, H., 2005. Anal. Chem. 77 (24), 8068–8074.
Lvov, Y., Decher, G., Sukhorukov, G., 1993. Macromolecules 26 (20), 5396–5399.
Lvov, Y.M., Lu, Z., Schenkman, J.B., Zu, X., Rusling, J.F., 1998. J. Am. Chem. Soc. 120 (17), 4073–4080.
Nadzhafova, Q.Y., Zaitsev, V.N., Drozdova, M.V., Vaze, A., Rusling, J.F., 2004. Electrochem. Commun. 6 (2), 205–209.
Nuthakki, B., Rusling, J.F., 2005. J. Electroanal. Chemi. 581 (1), 139–144.
Peng, S., Gao, Q., Wang, Q., Shi, J., 2004. Chem. Mater. 16 (13), 2675–2684.
Rosevear, A., Kennedy, J.F., Cabral, J.M.S., 1987. Immobilized Enzymes and Cells. Adam Hilger, Philadelphia.
Salimi, A., Sharifi, E., Noorbakhsh, A., Soltanian, S., 2006. Electrochem. Commun. 8 (9), 1499–1508.
Shchukin, D.G., Shutava, T., Shchukina, E., Sukhorukov, G.B., Lvov, Y.M., 2004. Chem. Mater. 16 (18), 3446–3451.
Topoglidis, E., Astuti, Y., Duriaux, F., Gratzel, M., Durrant, J.R., 2003. Langmuir 19 (17), 6894–6900.
Trindade, T., O'Brien, P., Pickett, N.L., 2001. Chem. Mater. 13 (11), 3843–3858.
Yamazaki, I., Araiso, T., Hayashi, Y., Yamada, H., Makino, R., 1978. Adv. Biophys. 11, 249–281.
Yap, F.L., Zhang, Y., 2007. Biosens. Bioelectron. 22 (6), 775–788.
Zhang, J.Z., 2000. J. Phys. Chem. B 104 (31), 7239–7253.
Zhao, G., Feng, J.J., Xu, J.J., Chen, H.Y., 2005. Electrochem. Commun. 7 (7), 724–729.
Zhou, H., Gan, X., Liu, T., Yang, Q.L., Li, G.X., 2006. Bioelectrochemistry 69 (1), 34–40.
Zhu, H., Stein, E.W., Lu, Z., Lvov, Y.M., McShane, M.J., 2005. Chem. Mater. 17 (9), 2323–2328.